DOI: 10.1002/adma.200701018

Fault-Tolerant Dielectric Elastomer Actuators using Single-Walled Carbon Nanotube Electrodes**

By *Wei Yuan*, *Liangbing Hu*, *Zhibin Yu*, *Tuling Lam*, *James Biggs*, *Soon M. Ha*, *Dongjuan Xi*, *Bin Chen*, *Matthew K. Senesky*, *George Grüner*, and *Qibing Pei**

Certain dielectric elastomers such as the 3M VHB 4910 acrylic adhesive films have exhibited electrically induced strains as high as 380 % in area expansion. The calculated maximum specific energy density of 3.4 J g^{-1} and maximum stress of 8 MPa are attractive for a wide range of applications including robotics, prosthetic devices, medical implants, pumps, and valves.[1–6] However, the performance of actuators based on the VHB films is substantially lower than the calculated values which reflect the maximum intrinsic material properties. Defects in the soft dielectric films, such as gel particles, uneven thickness, non-uniform crosslinking, and stress concentration, are possible causes for the reduced actuator performance. They also reduce the actuator reliability, hindering technology commercialization.[5,6] We introduce self-clearable compliant electrode materials that could enhance the fault-tolerance of the dielectric elastomers actuators. Thin metallic layers (10–100 nm) are being used for polypropylene thin-film capacitors for fault-tolerance. The electrode materials locally evaporate, or self-clear, around defects during high-voltage breakdown.[7–9] Metallic films are not sufficiently compliant for the dielectric elastomers. To enhance the compliancy of metallic electrodes, zig-zag shaped metallic lines were used to obtain 80 % area strains.[10] Uniform metallic coatings on corrugated silicone elastomer surfaces supported linear strains up to 33 %.[11] The commonly used compliant electrode materials for the VHB elastomers are powdered carbon graphite, carbon black, or carbon fibrils dispersed in grease or silicon oil, and electrolyte solutions.[12] No self-clearing has been reported for these electrode materials. Our experiments showed that single-walled carbon nanotubes (SWNTs) can overcome this morass. The SWNT electrodes have exhibited flexibility as transparent electrodes in light-emitting diodes, solar cells, and thin-film transistors.[13–16] With thin SWNT electrodes, the dielectric elastomer can not only be strained larger than 200 % in area expansion, but can achieve fault-tolerance through localized degradation of SWNTs.

Figure 1 shows a 300 % biaxially prestrained VHB 4910 film (62 μm thick after prestrain) with the SWNT electrodes at rest (Fig. 1a) and during actuation at 5 kV (Fig. 1b). The calculated strain is 200 %. This value is comparable with the same film using conventional carbon grease electrodes. The observed strain for 300 % biaxially prestrained VHB 4905 films (31 μm thick after prestrain) was 190 % at 3.5 kV.

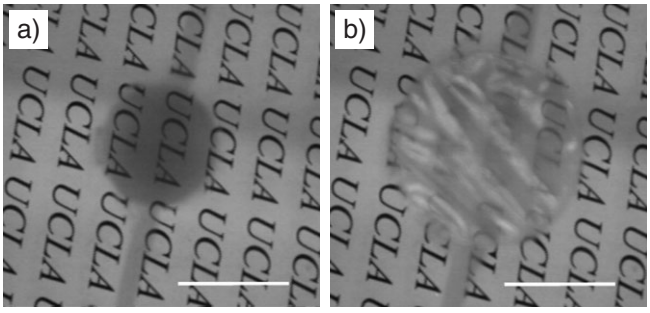

Figure 1. Circular strain test measuring the expansion of a 300 % biaxially prestrained VHB 4910 film with SWNT electrodes on both surfaces. The photo shows a 200 % area strain obtained from a) no voltage applied, and b) voltage at 5 kV. The scale bars are 10 mm.

The thickness of the SWNT electrodes greatly affects the obtained strain. Figure 2 shows the strain as a function of the applied voltage for different thicknesses of SWNT on a 300 % biaxially prestrained VHB 4905 film. For comparison, equal thicknesses of SWNT were applied on the two surfaces of each acrylic elastomers film. The surface resistances were 0.1, 0.2, 0.4, 4, and 20 kΩ $square^{-1}$, corresponding to calculated SWNT thicknesses of 250, 125, 60, 15, and 5 nm, respectively. For the calculation, see the Experimental section and Ref. [17].

Figure 2 shows a general trend of reduced strain at the same bias voltage with increasing thickness of the SWNT electrodes. This is probably due to increased stiffness of the electrodes. Strain in the dielectric elastomer films occurs owing to

[*] Prof. Q. Pei, W. Yuan, Z. B. Yu, T. Lam, S. M. Ha, D. J. Xi
Department of Materials Science and Engineering
University of California
Los Angeles, CA 90095 (USA)
E-mail: qpei@seas.ucla.edu
Prof. G. Grüner, Dr. L. B. Hu
Department of Physics and Astronomy
University of California
Los Angeles, CA 90095 (USA)
Dr. J. Biggs, Dr. M. K. Senesky
Artificial Muscle, Inc
Menlo Park, CA 94303 (USA)
Dr. B. Chen
NASA Ames Research Center
Moffett Field, CA 94035 (USA)

[**] This material is based upon work supported by the National Science Foundation under Grant No. 0507294 and DMR-0404029.

ADVANCED MATERIALS

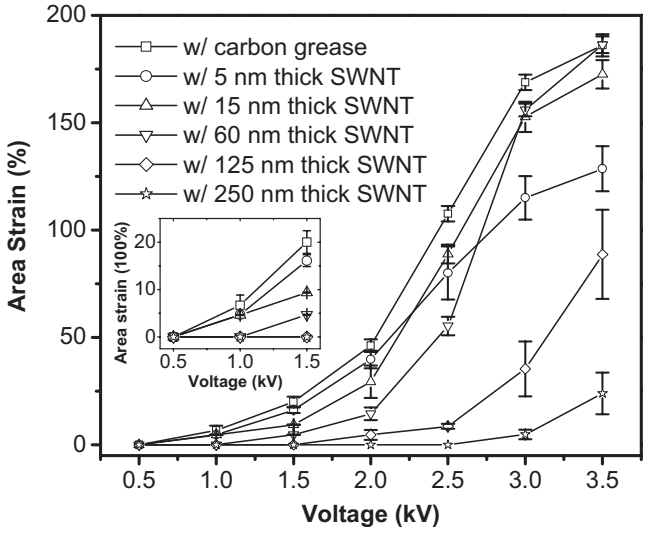

Figure 2. Electrically induced strain as a function of applied voltage on a 300 % biaxially prestrained VHB 4905 film with smeared carbon grease or SWNT electrodes on both surfaces. The SWNT electrodes have different thicknesses, as indicated in the inset. The inset figure zooms in the data points from 0.5 kV to 1.5 kV. For each SWNT thickness, three samples were tested. Each sample was actuated for 1 cycle at each 0.5 kV increment from 0.5 kV to 3.5 kV. Error bars indicate standard deviation.

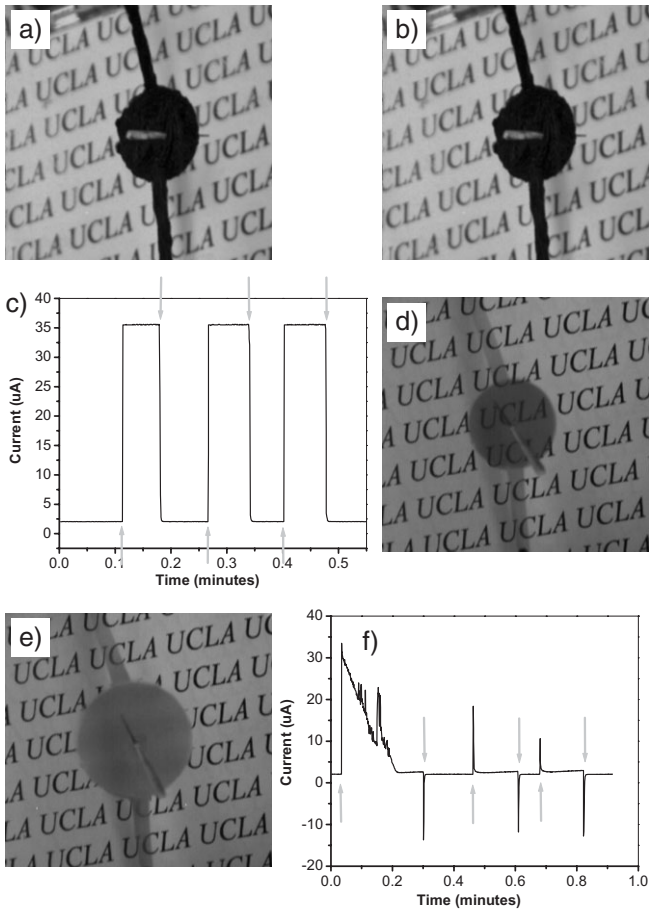

Figure 3. Fault-tolerance demonstration on a 200 % biaxially prestrained VHB 4905 film with either smeared carbon grease or SWNT electrodes and the actuation voltage is 3 kV. a,b) No strain was obtained once the fault was introduced to the device with carbon grease electrodes by a pin. c) The corresponding characteristic current–voltage curve of the shorted device for three actuations. The upward arrows indicate voltage application; the downward arrows indicate voltage turned off. d,e) 80 % strain was obtained on the film with SWNT electrodes through self-clearing, albeit a fault has been introduced. f) The current–voltage curve for the film with SWNT electrodes for three actuations. The first peak corresponds to the clearing event from the fault. The upward arrows indicate voltage application; the downward arrows indicate voltage turned off.

attraction of opposite charges across the dielectric film and repulsion of similar charges on each electrode.[2,4] This electrostatic force overcomes the elastic stress of the dielectric films, causing the sandwiched structure to shrink in thickness and expand in area. Stiffer, thicker electrodes may increase the elastic stress of the sandwich structure and impede the resulting strain. This explains why the films with 250 and 120 nm thick SWNT electrodes display lower actuation strain.

The samples with 5 nm thick SWNT electrodes show relatively high strain at low voltages until 2.0 to 2.5 kV, when the pace of strain increase with bias voltage wanes. Measurement of surface resistance showed that electrodes started to lose electrical connectivity, that is, the resistance became too high to measure with a multimeter, at strains greater than 100 %. On the other hand, the 15 and 60 nm thick SWNT electrodes can support higher strains. The 190 % strain of the 60 nm thick SWNT at 3.5 kV is comparable to that of carbon grease electrodes at the same bias. The 60 nm thick SWNT electrodes were thus chosen in the following fault-tolerance studies.

To demonstrate fault-tolerance enabled by the SWNT electrodes, a fault was intentionally introduced in 200 % biaxially prestrained VHB 4905 films by puncturing with a wood pin. Results from the measured strain response of the films after the puncturing are shown in Figure 3 for carbon grease electrodes and SWNT electrodes. The results for carbon grease electrodes are for comparative purpose and will be discussed first.

Before a fault was introduced, the film with carbon grease electrodes was strained to 125 % at 3 kV while the film with SWNT electrodes was strained to 100 % at the same voltage. The difference in the observed strain is consistent with the results shown in Figure 2. After the acrylic film coated with carbon grease electrodes was punctured with a pin, no strain was observed at high field (Fig. 3a and b). The current–voltage curve shown in Figure 3c indicates a short in the circuit. The maximum current when voltage was applied is limited by the current-limiting resistor. When the voltage was turned off, no current pulse from discharge was observed, indicating no charge storage and, hence, a short circuit in the acrylic film. The introduced fault is thus permanent.

When the acrylic film coated with SWNT electrodes was punctured with the pin, a clearing process occurred around the puncture. The clearing process, characterized by a brief display of electric sparks, was initiated by the puncture of the

acrylic film. As indicated in Figure 3d and e, an 80 % calculated actuation strain was achieved upon completion of the clearing process. Excluding the cleared, non-active area, the actuation strain was about 100 %. A stable strain was successfully maintained at a voltage of 3 kV. Normal actuation of the punctured film was attained in subsequent intermittent application of voltage regardless of the presence of the pin.

The current–voltage curve in Figure 3f shows the sparking event during the first voltage application when the film was punctured. The current, which was limited by the series of resistors, peaked to 35 μA, then decreased steadily from 30 μA to 3 μA in 10 s. After the sparking event ceased, the actuation strain reached a steady state value of 80 %, with normal actuation. The current–voltage response after the clearing peak thus resumed the characteristic charging and discharging behaviors before puncturing.

This fault-tolerance using SWNT electrodes is attributed to localized electrode degradation around the puncture fault by electric arc. The circular area centered at the fault consequently becomes non-conductive, extending outwards. Figure 4a, a scanning electron microscopy (SEM) image, shows the SWNT network in the electrode. Figure 4b shows isolated patches of SWNT caused by partial removal from electric arc in the degraded area. The presence of the radical breathing mode on the Raman spectra taken from the cleared area, albeit with slightly lower intensity compared with the uncleared area, further confirmed the partial removal of SWNT.[18] These patches, which consist of intact networks of SWNTs, are electrically isolated from each other and thus do not form a conductive path. The nonconductive paths between the patches consist only of scattered SWNT and the exposed acrylic film. The punctured fault is thus isolated from the rest of the active area. This accounts for the fault tolerance of SWNT-based dielectric elastomer actuators.

The degradation of SWNTs has been reported under high current as a field emitter,[19–21] under high temperature as a light bulb filament,[18] or under plasma.[22] The fluffy SWNTs can be even ignited in air with a 100 mW cm^{-2} photographic flash.[23] The instability of the SWNT under these harsh conditions has been attributed to the bent tube structure and the single wall layer.[24,25] In the fault-tolerance experiment described above, the current rose to 35 μA. Much of this current passed through a very small area over which the electrical heating may be significant because of the high voltage applied. The elevated temperature, high enough to burn a hole through the acrylic film, caused arcing and degradation of the SWNT. From Figure 4b, the degradation occurred through narrow pathways until the area became too resistive to sustain the arcing.

Soft dielectric elastomers generally contain various structural defects, such as gel particles, embedded foreign particles, and non-uniform crosslinking which lead to the non-uniform distribution of stiffness, non-uniform film thickness, and the attachment of foreign particles on the film surface. All of these defects may cause dielectric breakdown at an electric field substantially lower than that the intrinsic polymer can sustain. The self-clearable SWNT electrodes were studied to prevent premature failure when such breakdown occurs. For this purpose, VHB 4910 acrylic films, which were 300 % biaxially prestrained and coated with thin SWNT electrodes of 60 nm thickness, were actuated with voltage increments of 0.5 kV starting from 3 kV until the films ruptured and terminally failed.

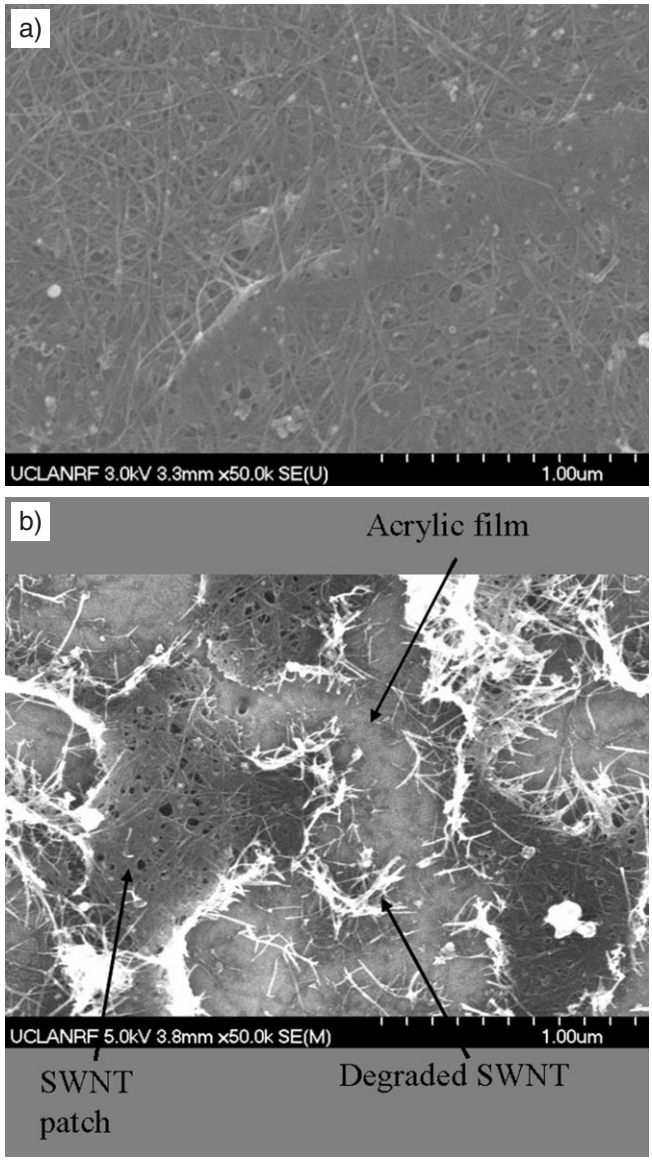

Figure 4. SEM images of a) the SWNT electrode surface before voltage application, and b) the self-cleared SWNT electrode surface near the fault.

The chronoamperic responses (*I–t*) at 6 kV and above are shown in Figure 5a. At 7 kV and below, no clearing event was observed. The *I–t* curve at each increment only exhibits the initial charging current pulse followed by a relatively steady state current (discharging pulses were not shown in this figure). The clearing event, which occurred at 7.5 kV in 2.5 s, is characterized by a large current spike. After clearing finished,

ADVANCED MATERIALS

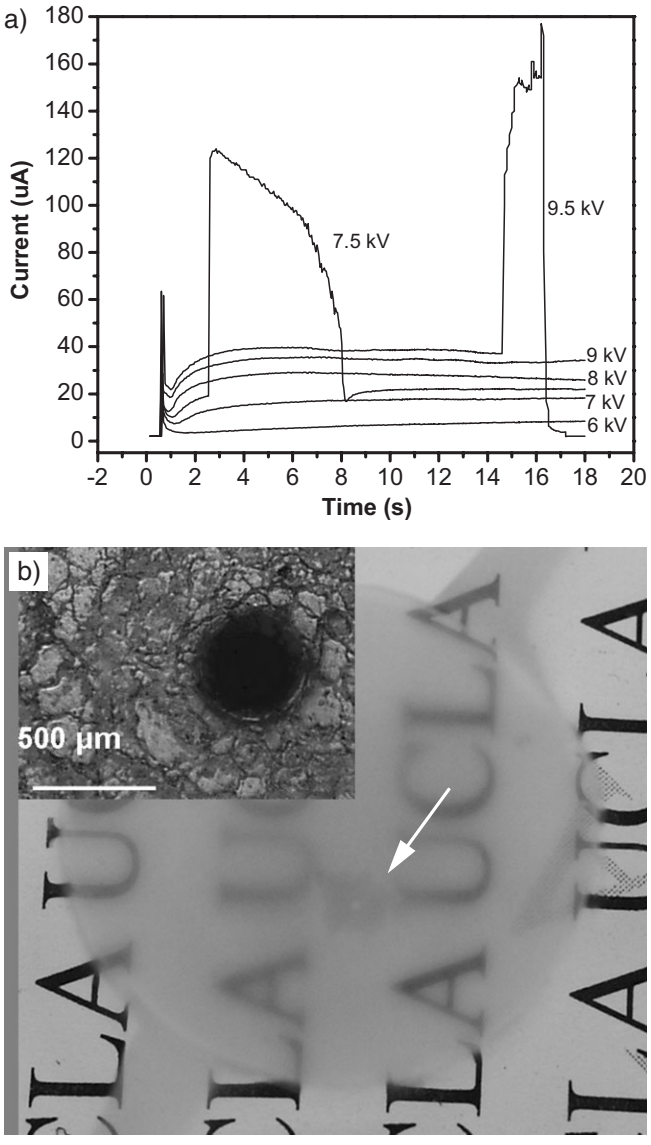

Figure 5. Demonstration of the clearing event preventing the premature failure of film during actuation with increased voltage. a) Chronoamperic curves of the actuation at increasing voltages from 6 kV to 9.5 kV with increasing increments of 0.5 kV (6.5 kV and 8.5 kV did not show in this figure). The spike in the 7.5 kV curve characterized clearing event. b) The arrow indicates the site of corresponding clearing event in the film (figure size is 55 × 55 mm^2), and Inset: image further showing the dielectric breakdown hole as well as damaged SWNT electrode.

the diminished current turns to slightly increasing with time while the active area of the film expanded from 0 to 150 % strain. The corresponding clearing area shown in Figure 5b (indicated with the arrow) is a circle with a diameter of 4 mm. The size of this spot remained unchanged during the rest of the actuation at 7.5 kV. Further examination of the cleared area revealed a hole through the film with a 300 µm diameter (inset in Fig. 5b), formed from the dielectric breakdown.

As the voltage was raised to 8 kV, 8.5 kV, and 9 kV, no additional clearing event occurred. The actuation strain increased to 230 % at 9 kV. At 9.5 kV, a new clearing event occurred in a different location after the film was actuated for 14 s at this voltage. During this clearing event, the current was rather high and the breakdown-induced hole rather large, such that the film mechanically ruptured before the clearing was completed. Note that the film before rupturing was under high tension.

When the clearing occurred at 7.5 kV, the electric field in the acrylic film was 240 V μm^{-1}, a value slightly higher than the measured dielectric strength based on rigid brass electrodes.[26] After this clearing event, the dielectric strength of the remaining active area increased to 340 V μm^{-1}. This value is at the high end of the reported dielectric strengths for the same acrylic films under high electric strain.[4,27] The SWNT electrodes do not alter the intrinsic dielectric strength of the acrylic polymer, but effectively prevent premature dielectric failure caused by defects. This leads to the enhancement of dielectric strength and attainable strain over large-area films and to possible improvement in actuator reliability.

We have shown that thin SWNT electrodes are self-clearable and compliant to drive dielectric elastomers. The instability of the SWNT at the dielectric breakdown (arcing) condition caused its localized degradation and loss of conductivity around the breakdown site. This SWNT self-clearing isolates the fault from the rest of the active area which can actuate normally. The fault-tolerant dielectric elastomers exhibit an electrically induced strain comparable to those based on conventional compliant electrode materials such as carbon grease. Furthermore, the probability of terminal failure caused by defects is significantly reduced. Studies are ongoing to evaluate how the SWNT electrode responds to high frequency driving and whether it prolongs the operation lifetime of dielectric elastomer actuators.

Experimental

Purified P3 SWNTs (Carbon Solution, Inc.) were dispersed in an aqueous solution at 2 mg mL^{-1} through sonication [17] and sprayed onto acrylic elastomer films (3M VHB adhesive tapes, biaxially prestrained) using an airbrush (Paasche Airbrush Company). The spraying rate was controlled at 1 mL min^{-1}. Coating thickness was monitored by measuring film surface resistance with two concentric brass probes, R_{outer} = 0.585" and R_{inner} = 0.185". The probes were placed on the coated films laminated onto rigid pizza papers. The thickness t is estimated using $t = 1/R_s s$, where R_s is the surface resistance and s is the conductivity of P3 film and equals to 400 S cm^{-1}. To σ value was measured on coatings sprayed onto transparency film and found consistent with Ref. [17]. Thicknesses 50 nm or greater were found comparable with cross-sectional imaging by scanning electron microscopy. The overlapped circular areas of SWNT electrodes with electrical leads were sprayed on both surfaces of each acrylic film through a contact mask (see Fig. 1a). High voltage was applied via the two electrical leads to actuate the SWNT/acrylic/SWNT sandwich structure.

For fault-tolerance demonstration and self-clearing with incremental voltage, biaxially prestrained acrylic films coated with electrodes on both surfaces were connected in series with 50–80 MΩ current-limiting resistors, Keithley 2000 multimeter, and a high-voltage power supply. The current-limiting resistors were used to protect the highly prestrained acrylic film from rupture in case of high current. The chronoamperic curve was obtained by the Keithley 2000 multimeter controlled by LABView software.

Area expansions of the films were recorded by a digital camera. The area strain was obtained through $\frac{a_1-a_0}{a_0}\cdot 100\,\%$, where a_1 is the actuated area under high voltage, and a_0 is the area at 0 kV. For films undergone self-clearing, the cleared circular areas around defects were subtracted from both a_1 and a_0.

The electrical field was calculated through

$E=\frac{HV-U_{resistor}}{d}=\frac{HV-IR}{d_0/S+1}$, where HV is the high voltage from the high voltage supply; U_{resistor} is the voltage dropped on the current-limiting resistor, and equal to IR, where I, the current recorded by the multimeter, and R, the resistance of the current-limiting resistor; and d is the film thickness and equal to prestrained film thickness divided by area expansion (S+1) with the assumption that the acrylic films are incompressible.

Received: April 28, 2007
Revised: August 10, 2007
Published online: January 17, 2008

[1] *Electroactive Polymer (EPA) Actuators as Artificial Muscles: Reality, Potential, and Challenge*, 2nd ed. (Ed: Y. Bar-Cohen), SPIE, Bellingham, WA **2004**.
[2] R. Pelrine, R. Kornbluh, G. Kofod, *Adv. Mater.* **2000**, *12*, 1223.
[3] Q. Pei, M. Rosenthal, S. Stanford, H. Prahlad, R. Pelrine, *Smart Mater. Struct.* **2004**, *13*, N86.
[4] R. Perine, R. Kornbluh, Q. Pei, J. Joseph, *Science* **2000**, *287*, 836.
[5] R. Kornbluh, *Mater. Technol.* **2004**, *19*, 216.
[6] Q. Pei, R. Pelrine, S. Stanford, R. Kornbluh, M. Rosenthal, *Synth. Met.* **2003**, *135*, 129.
[7] C. W. Reed, S. W. Cichanowski, *IEEE Trans. Dielectr. Electr. Insul.* **1994**, *1*, 904.
[8] H. Heywang, *Colloid Polym. Sci.* **1976**, *254*, 138.
[9] J. H. Tortai, N. Bonifaci, A. Denat, *J. Appl. Phys.* **2005**, *97*, 053304.
[10] R. Pelrine, R. Kornbluh, J. Joseph, R. Heydt, Q. Pei, S. Chiba, *Mater. Sci. Eng. C* **2000**, *11*, 89.
[11] M. Benslimane, P. Gravesen, P. Sommer-Larsen, *Proc. SPIE-Int. Soc. Opt. Eng.* **2002**, *4695*, 150.
[12] F. Carpi, P. Chiarelli, A. Mazzoldi, D. D. Rossi, *Sens. Actuators A* **2003**, *107*, 85.
[13] Q. Cao, Z. T. Zhu, M. G. Lemaitre, M. G. Xia, M. Shim, J. A. Rogers, *Appl. Phys. Lett.* **2006**, *88*, 113511.
[14] T. Takenobu, T. Takahashi, T. Kanbara, K. Tsukagoshi, Y. Aoyagi, Y. Iwasa, *Appl. Phys. Lett.* **2006**, *88*, 033511.
[15] M. W. Rowell, M. A. Topinka, M. D. McGehee, H. Prall, G. Dennler, N. S. Sariciftci, L. Hu, G. Gruner, *Appl. Phys. Lett.* **2006**, *88*, 233506.
[16] R. Ulbricht, X. Jiang, S. Lee, K. Inoue, M. Zhang, S. Fang, R. Baughman, A. Zakhidov, *Phys. Status Solidi B* **2006**, *243*, 3528.
[17] E. Bekyarova, M. E. Itkis, N. Cabrera, B. Zhao, A. Yu, J. Gao, R. Haddon, *J. Am. Chem. Soc.* **2005**, *127*, 5990.
[18] Z. G. Zhao, F. Li, C. Liu, H. M. Cheng, *J. Appl. Phys.* **2005**, *98*, 044306.
[19] J. M. Bonard, C. Klinke, K. A. Dean, B. F. Coll, *Phys. Rev. B* **2003**, *67*, 115406.
[20] J. M. Bonard, J. P. Salvetat, T. Stockli, W. A. de Heer, L. Forró, A. Châtelain, *Appl. Phys. Lett.* **1998**, *73*, 918.
[21] Y. Wei, C. Xie, K. A. Dean, B. F. Coll, *Appl. Phys. Lett.* **2001**, *79*, 4527.
[22] G. Zhang, P. Qi, X. Wang, Y. Lu, X. Li, R. Tu, S. Bangsaruntip, D. Mann, L. Zhang, H. Dai, *Science* **2006**, *314*, 974.
[23] P. M. Ajayan, M. Terrones, A. de la Guardia, V. Huc, N. Grobert, B. Q. Wei, H. Lezec, G. Ramanath, T. W. Ebbesen, *Science* **2002**, *296*, 705.
[24] P. G. Collins, M. S. Arnold, P. Avouris, *Science* **2001**, *292*, 706.
[25] D. J. Mann, W. L. Hase, *Phys. Chem. Chem. Phys.* **2001**, *3*, 4376.
[26] G. Kofod, R. Kornbluh, R. Pelrine, P. Sommer-Larsen, *Proc. SPIE-Int. Soc. Opt. Eng.* **2001**, *141*, 4329.
[27] S. M. Ha, W. Yuan, Q. B. Pei, R. P. Pelrine, S. Stanford, *Adv. Mater.* **2006**, *18*, 887.

